Energy-based analytical formulation for the prediction of end debonding in strengthened steel beams

Massimiliano Bocciarelli, Pierluigi Colombi *, Giulia Fava, Lisa Sonzogni

Department of Architecture, Built Environment and Construction Engineering (ABC), Politecnico di Milano, P.zza L. da Vinci, 32 – 20133 Milan, Italy

This paper deals with the evaluation of the edge bond strength of steel beams retrofitted with Fibre Reinforced Polymer (FRP) materials. Two approaches were mainly investigated, that is the stress-based criterion and the energy-based one. The latter is simpler since it does not require assessing the mechanical and geometrical properties of the adhesive layer. The basic concept is that fracture occurs when the strain energy release rate (SERR) reaches a critical value. Then, a simplified and general-purpose energy-based analytical formulation is proposed to indirectly estimate the SERR. Actually, several linear and non-linear methods allow analysing the end debonding failure. However, such models are often difficult to develop, not immediate and a considerable calculation effort is needed. Therefore, the formulation discussed in this paper was proposed for being straightforwardly applied in the design phase of reinforced steel beams under general loading configurations and static schemes. To validate the analytical approach, experimental results for a simply supported beam are considered. A parametric analysis is also performed and the results are compared to the ones of a recently proposed numerical method. A good agreement among the experimental, analytical and numerical models was found in all the cases, showing the potentialities of the proposed approach.

Keywords:
FRP materials
Bond strength
Interfacial crack model
Fracture energy
Steel beams

1. Introduction

Civil structures may become inadequate for several reasons, e.g. design errors, material degradation and variation of the load acting on the structures. In particular, steel structures are sensitive to fatigue and corrosion, leading to a drastic reduction of their load bearing capacity. Standard rehabilitation techniques make use of welded or bolted steel plates to reinforce the damaged elements but the problem of steel corrosion still remains and difficulties in fitting complex profiles can arise.

Fibres Reinforced Polymer (FRP) materials and in particular CFRP (Carbon Fibres Reinforced Polymer) materials were proposed in the past to retrofit concrete and masonry structures [1,2], due to their well-known high mechanical properties and the very low dead weight. Despite their high intrinsic cost, the possibility to shape the FRP materials and to avoid the cumbersome work associated to standard reinforcement techniques makes the global rehabilitation cost acceptable. These techniques were also proposed to reinforce steel structures [3]. For instance, the retrofitting of existing steel beams, by bonding a CFRP plate to the tension flange, increases both the local stiffness (while the global stiffness increment is in general marginal) and the flexural capacity [4–6]. The local stiffness increment achieved is very important from the fatigue point of view, see [7–14]. Design criteria [15] and design guidelines were also released, see [16,17], to help engineers in the use of FRP materials to retrofit damaged steel structures.

1.1. Problem statement

In steel beams strengthened by bonding CFRP materials to the tension flange, collapse is mainly due to the CFRP strip debonding or to the carbon reinforcement failure [18]. Debonding of the CFRP plate is the main failure mode and it prevents the achievement of the full flexural capacity of the composite section [16]. Debonding always takes place in a stress concentration region and it is due to an interface crack initiation and propagation in the adhesive layer or at the interface between the adhesive and the substrate. In reinforced steel structures, the crack does not occur in the substrate as it does in retrofitted concrete elements. Besides, collapse is a very brittle and highly instable phenomenon and, for this reason, the relevant bond strength is determining from the design point of view. In the literature [5], an outstanding attention was dedicated to such failure mode due to the need of a reliable predicting model

* Corresponding author.
E-mail address: pierluigi.colombi@polimi.it (P. Colombi).

Published Journal Article available at: http://dx.doi.org/10.1016/j.compstruct.2016.05.084

for design purposes. In reinforced steel beams, debonding may take place at the reinforcement ends or at plastic hinge location [16]. In the first case, stress concentration is due to a geometric discontinuity at the reinforcement end, while in the second case interface stress concentration arises in view the local high curvature value following the formation of the plastic hinge, strictly dependent on the elasto-plastic behaviour assumed for steel, see [6,19–21]. In what follows, reference is made to edge debonding occurring at the reinforcement end, where an elastic strain–stress relation-ship can be always considered for steel.

For sake of simplicity, interface normal stresses (peeling) are usually neglected [22]. This means that the adhesive acts as a shear lag between the beam and the reinforcement.

The first method proposed in the literature for the evaluation of the bond strength at the reinforcement ends is the so-called stress-based approach. The main advantages of this approach are related to capability of the method to automatically detect the crack initiation point and the direction of crack propagation. For a linear interface behaviour, it assumes that debonding takes place when the interface stresses, responsible for the combined action of steel beam and reinforcement, exceed a critical threshold [16,22,23]. The main disadvantage of the stress-based approach is related to the definition of the adhesive geometrical (thickness) and mechan-ical (shear modulus) properties. These parameters generally pre-sent a large variability and the bond strength, evaluated in terms of stress analysis results, is subjected to a great uncertainty [16]. For a non-linear adhesive behaviour, the maximum load should be detected from the complete equilibrium path of the plated steel beam [24] and the main disadvantages of this approach are related to the required computational effort and the uncertainty in the def-inition of the non-linear material parameters.

As an alternative approach, the fracture mechanics energy-based criterion was proposed in the literature [25–28]. In this method, the bond strength is assessed on the basis of the energy released at the interface during debonding. The associated failure criterion states that the interfacial crack propagates if the SERR is greater than a critical value, G_c, which is a property of the interface. The evaluation of the SERR requires at first the computation of the strain energy for the whole structure and then its derivative with respect to the crack area [24]. Both tasks require a numerical solu-tion even though very simple beam configurations (simply sup-ported beam) and loading scheme are considered.

The main advantage of the energy-based approach is the linearity while the disadvantage is the need of a qualitative description of the interface crack growth mechanism. Finally, only the value of the fracture energy G_c is required to characterize the interface behaviour. In fact, the crack initiation point and the direction of crack propagation need to be specified in advance.

Another way to model edge debonding is provided by the cohesive zone modelling approach. This technique has been extensively used to analyse general fracture phenomena under static, dynamics and cyclic loading [29] and debonding in tensile steel/CFRP joints [30–33]. In the cohesive zone approach, a bond-slip law relationship is assumed between the interfacial stresses and the relative displacements at the interface.

1.2. Scope of the research

The aim of the paper is to propose a general purpose energy-based method for estimating the edge bond strength of CFRP reinforced steel beams. Such a simplified formulation is proposed to be used in the design phase of strengthened metallic members. As previously observed, several methods are discussed in the literature to estimate the end debonding failure in strengthened steel beams and to analyse the interfacial behaviour capturing both linear and non-linear effects. On the other hand, the existing models are often difficult and cumbersome to develop and a considerable calculation effort is required. For this reason, the method herein presented aims to provide a reliable and simple estimation of the end debonding strength with an immediate and correct understanding of the parameters involved in the design of reinforced steel beams. As a result, the formulation discussed is proposed for being straightforwardly applied in the design phase of rein-forced steel beams under general loading configurations and static schemes.

The proposed energy-based approach is composed of two stages. In the first step, the stresses in the adherents and in the adhesive layer are assessed. In the second step, the SERR is evalu-ated and compared to its critical value in order to calculate the bond strength. The stress analysis phase is relatively simple from the analytical point of view and capable to capture the main fea-tures of the problem. Additionally, the second phase avoids the cumbersome work associated to a numerical evaluation of the SERR.

A simplified one-parameter shear lag model (i.e. no peeling stresses are considered) is introduced to perform the stress analysis phase of the energy-based criteria. Besides, an indirect method for the calculation of the SERR avoiding the numerical evaluation in the derivative of the complementary strain energy with respect to the crack area is adopted. The results of the proposed method are firstly validated through the comparison with experimental results related to CFRP strengthened steel beams. Then it is shown that the proposed simplified shear lag model could be applied to general loading configurations and static schemes. This will be proven numerically, without any loss of generality, for a simply supported beam under different loading configurations using a recently proposed numerical method [34] for the evaluation of the bond strength of plated beam.

This represents a significant improvement of the analytical results available in the literature since they are very often limited to the case of a simply supported beam under three-point bending loading configuration.

1.3. Previous studies

In the literature stress-based criteria for the end debonding of CFRP reinforced steel beams were firstly proposed [16]. Elastic analysis of steel beams reinforced by CFRP strips is usually adopted for the evaluation of interfacial stresses. In [22] a closed-form expression was developed for the elastic shear and peel stresses in the adhesive layer of a strengthened beam, allowing loading, temperature effects and composite strips pre-strain to be considered in the design. Shear and peel stresses were then inserted into a stress-based criterion to assess the load carrying capacity of the adhesive layer.

Deng and Lee [23] developed theoretical analyses for estimating the maximum interfacial stresses at the plate end as well as the longitudinal stress in the CFRP strip. Experimental tests were also performed for evaluating the effects of tapered plates and of the spew fillet in the adhesive.

Alternatively, fracture mechanics concepts were used to investigate the end debonding of CFRP reinforced steel beams. As an example, in [25] the virtual crack extension (VCE) method was adopted in conjunction with simplified models for the stress analysis of reinforced beams and a numerical approximation of the SERR was finally attained. The following stress analysis techniques were discussed: equivalent beam model, one-parameter model, two-parameter model and higher order model. They correspond to an increasing accuracy but also to a growing complexity. In the equivalent beam model, perfect bonding between the adher-ents is considered. This method roughly approximates the inter-face behaviour but it was often adopted [26,27] since it leads to

a very simple design formula for the maximum bending moment, $M_{0,\max}$, at the reinforcing end:

$$M_{0,\max} = \sqrt{\frac{2G_c b_f}{\frac{1}{E_s I_s} - \frac{1}{E_s I_r}}} \quad (1)$$

where G_c is the fracture energy, E_s is the Young's modulus of the steel beam, b_f is the reinforcement width and I_s and I_r are the moments of inertia of the unreinforced steel beam and of the reinforced homogenised one, respectively. In the literature, Eq. (1) is sometimes referred as the linear elastic fracture mechanics (LEFM) solution to the edge debonding of plated beams [16,35]. In the one-parameter model, the adhesive shear stress is considered while the peeling stress is neglected. The adhesive layer is then regarded as an elastic foundation with horizontal springs. This is a reasonable assumption since the load is transferred from the beam to the CFRP reinforcement by the adhesive shear stress. Such model is relatively simple and capable to capture the main features of the problem [27,36] and to provide useful design formulae for the edge debonding investigation. The two-parameter model considers both shear and peeling stresses at the interface, that is the adhesive layer is considered as an elastic foundation with horizontal and vertical springs. Since the horizontal and vertical springs in the one-parameter and the two-parameter interface models represent the adhesive layer, they depend on both the adhesive mechanical and geometrical properties. In the high order model, the adhesive is modelled as an elastic continuum. The two-parameter model and the high order one are extremely accurate but do not provide a closed-form solution.

In [26] analytical and numerical models for the evaluation of the SERR in steel reinforced beams were proposed. The analytical models consist of a simplified version of the two-parameter model and the equivalent beam method while the numerical analyses refer to the modified virtual crack closure technique.

In [27] the edge debonding of FRP strengthened beams was investigated using both stress and energy-based approaches. It was concluded that the two methods are linked together by a sim-ple formula but the energy-based one is more effective to investi-gate edge debonding failure mode. The interface crack instability that may occur after the debonding onset was finally investigated.

In [36] a cohesive zone model of interfacial stresses in plated beams was proposed. A one-parameter model was implemented to capture the essential features of the problem and to provide a closed-form solution for the end debonding of reinforced beams. Analytical results were compared to the ones provided by an energy-based approach in conjunction to transformed section model. Comparison with numerical results was also performed.

Finally, in [37] debonding failure was investigated using finite element modelling. In particular, a mixed-mode cohesive law was proposed to analyse the interfacial behaviour under a combi-nation of mode-I and mode-II loading. The study revealed that the mode-I fracture energy has a marginal contribution in the defini-tion of the debonding load. Besides, when brittle adhesives are employed and end debonding is concerned, the values of the ulti-mate load and of the load related to debonding initiation are extre-mely close each other. Thus, the reinforced beam strength may be assumed to be equal to the load at which debonding is triggered.

2. Energy-based failure criterion for edge debonding

In this Section, the energy-based failure criterion is introduced with reference, for sake of simplicity but without any loss of generality, to the simply supported steel beam reported in Fig. 1.
The beam is reinforced with a CFRP plate bonded to the bottom side of the lower steel flange. The energy failure criterion for studying the end debonding of plated beams is based on the proposal of [16]. Since debonding is due to the interfacial crack initiation and propagation, the crack will grow if the energy released for a crack increment is equal or greater than the energy required to create a new crack surface. This very simple energy balance leads to the definition of the SERR, G, which is specific for the interface under analysis. Fracture occurs when the SERR is equal to its critical value, G_c. The SERR is a well-known fracture mechanics quantity [38] and it is defined on the basis of the above-mentioned energy balance as:

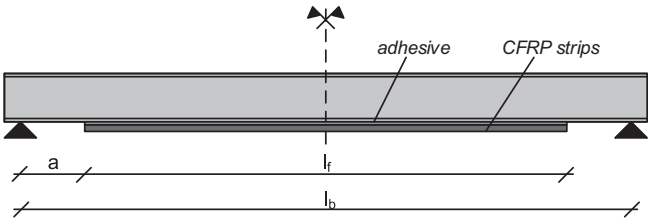

Fig. 1. Simply supported steel beam reinforced with a CFRP plate: beam geometry.

$$G = \frac{\partial U^*}{\partial A} = \frac{1}{b_f}\frac{\partial U^*}{\partial b} \quad (2)$$

where U^* is the complementary strain energy, b_f the CFRP width and b is the interface crack length. Since U^* is the whole comple-mentary energy of the plated beam, for computing its value both the stresses in the adherents (beam and CFRP plate) and in the adhesive layer are needed [26,27]. Two steps are then required for applying the energy failure criterion. At first the stresses in the adherents and in the adhesive layer are evaluated to calculate the complementary strain energy and then the SERR is computed from Eq. (2).

In this paper, from the stress analysis point of view, linear interface brittle behaviour is assumed and a one-parameter model is adopted to evaluate the stress in the adherents and in the adhesive. From the SERR point of view, since it is hard to analytically calculate the partial derivative of Eq. (2), it is preferred to adopt the VCE method [25] that numerically approximates the partial derivative of Eq. (2) by evaluating the complementary energy for two different but very close interface crack lengths.

In CFRP reinforced steel elements, the adhesive layer physically represents the interface since the failure mode does not involve the steel substrate. For a one-parameter stress analysis model, just the shear stress and the tangential relative displacement (mode-II) at the interface are considered, in fact the effects of the mode-I loading are usually negligible [37]. Different bond-slip relationships between the interface shear stress τ and the relative displacement δ are available in the literature. Among them, the most commonly used is the bilinear bond–slip relationship (see Fig. 2), that is [27,36]:

$$\tau = \begin{cases} k_1\delta & \text{for} \quad \delta \leqslant \delta_p \\ -k_2\delta + \tau_p\left(\dfrac{k_1+k_2}{k_1}\right) & \text{for} \quad \delta_p \leqslant \delta \leqslant \delta_u \\ 0 & \text{for} \quad \delta \geqslant \delta_u \end{cases} \quad (3)$$

The exponential bond–slip relationship (see Fig. 3) is also adopted in the literature [30,21], that is:

$$\tau = \delta\frac{\tau_p}{\delta_p}\left[\exp\left(1-\frac{\delta}{\delta_p}\right)\right] \quad (4)$$

In Eqs. (3) and (4), τ_p is the maximum shear stress, δ_p is the relative displacement at τ_p, δ_u is the ultimate relative displacement while k_1 and k_2 are the slopes of the elastic and the softening branch, respectively.

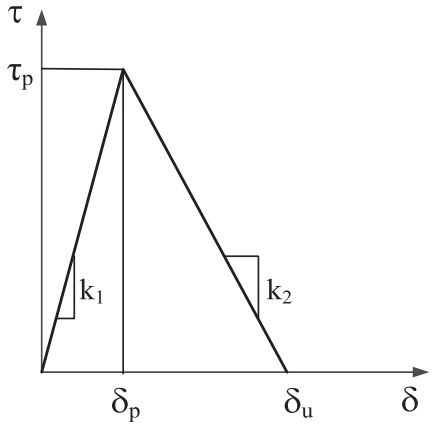

Fig. 2. Bi-linear interface bond–slip law.

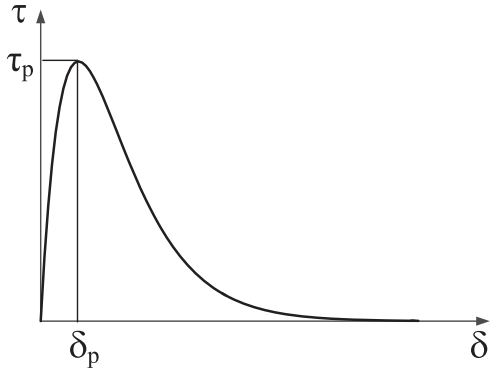

Fig. 3. Exponential interface bond–slip law.

Since the bond–slip law covers the entire interface behaviour up to the complete debonding, the area under the bond–slip law represents the energy spent to separate the adherents and to advance the interface crack. One has:

$$G_c = \int_0^{\infty} \tau d\delta \tag{5}$$

where G_c is the critical fracture energy at the interface. Considering the bond–slip relationships given in Eq. (3) and in Eq. (4), the integral in Eq. (5) can be easily performed and it provides, for the bilinear bond–slip relationship:

$$G_c = \mu \frac{\tau_p^2}{2k_1} \tag{6}$$

where $\mu = \delta_u/\delta_p$, while for the exponential bond–slip relationship one has:

$$G_c = e\delta_p\tau_p \tag{7}$$

Note that (see Fig. 4) the parameter μ controls the shape of the bilinear bond–slip curve in Eq. (3) and for $\mu = 1$ a brittle linear interface behaviour is achieved.

It should be finally pointed out that Eq. (6) bridges the gap between the stress-based approach and the energy-based one [36,27]. In particular, for $\mu = 1$ a relationship between the maximum shear stress at the interface and the SERR is provided:

$$G_c = \frac{\tau_p^2}{2k_1} \tag{8}$$

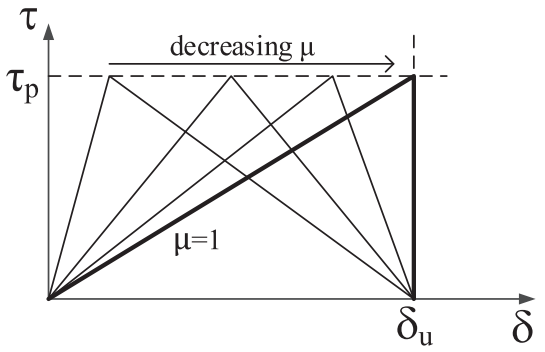

Fig. 4. Bilinear bond–slip relationship for different values of the parameter μ.

Eq. (6) can therefore be used to shift from a stress-based failure approach to an energy-based one avoiding the numerical approximation of the VCE method. This concept will be used in the next Section to derive a simplified energy-based analytical formulation for edge debonding.

In [36] a cohesive interface model was implemented to study a simply supported plated beam under three-point bending loading configuration (see Fig. 5):

The maximum load was computed as:

$$P_{\max} = \frac{2b_f f_2 E_s I_s}{y_s} \cdot \frac{\tau_p \sqrt{\mu}}{\lambda a + \sqrt{\mu}} \tag{9}$$

where $f_2 = 1/E_f b_f t_f$ (see Appendix A) and:

$$\lambda^2 = \frac{k_1}{E_f t_f} \tag{10}$$

while $\mu = \delta_u/\delta_f$ (see Fig. 4). In Eqs. (9) and (10), E_s and E_f are the steel and reinforcement Young's moduli, respectively, b_f is the reinforcing width, y_s is the distance of the centroid of the steel beam from the lower flange while τ_p is the maximum shear stress (see Fig. 2). Eq. (9) was obtained using a bilinear bond–slip law and then the different softening stages were considered for defining the equilibrium path and the maximum load. This is a quite complicated procedure even for a very simple beam geometry and loading configuration. Substituting Eq. (6) into Eq. (10), one has:

$$\lambda^2 = \frac{\tau_p^2 \mu}{2G_c E_f t_f} \tag{11}$$

Finally, inserting Eq. (11) into Eq. (9), the maximum load can be expressed as:

$$P_{\max} = \frac{2b_f f_2 E_s I_s}{y_s} \cdot \frac{\tau_p}{1 + \frac{\tau_p a}{\sqrt{2G_c E_f t_f}}} \tag{12}$$

which is independent from the shape of the bond–slip law since the ratio μ disappears. This means that the maximum load depends only on the fracture energy G_c and on the relevant maximum shear stress τ_p. From the numerical point of view, this was observed in

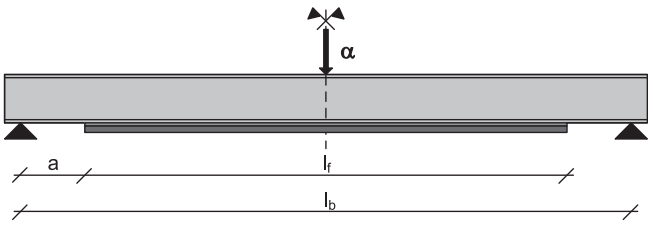

Fig. 5. Simply supported beam under three-point bending loading configuration.

[21] and [34] but it was never pointed out analytically. Besides, the dependency of the bond strength from the maximum shear stress is usually neglected in the design formulae.

3. A simplified energy-based analytical formulation for edge debonding

A simplified analytical formulation for edge debonding is summarized in the following while a detailed derivation is reported in Appendix A. The sign conventions and notations used in the formulation are reported in Fig. 6.

The main assumptions are:

- Elastic strain–stress relationship for the substrate and the composite strips;
- Linear elastic and brittle behaviour of the interface;
- Eulero–Bernoulli theory is used for the beam, that is plane sections remain plane and the shear deformation is neglected;
- Bending of the composite strips is neglected;
- The adhesive layer and its interfaces are modelled as a single interface;
- No peeling (normal stress) is considered at the interface, that is the interface (adhesive layer) acts as a shear lag and just the shear stress component is considered.

The longitudinal relative displacement across the interface, δ, is defined as:

$$\delta = u_{sa} - u_f \tag{13}$$

where u_{sa} and u_f are the longitudinal displacements of the beam at the steel/adhesive interface and of the composite strip, respectively. The longitudinal relative displacement across the interface, δ, can be re-written, making use of the kinematic relationship for the steel beam (plane sections remain plane):

$$\delta = u_s + \psi_s y_s - u_f \tag{14}$$

where ψ_s is the rotation of the section of the steel beam, u_s is the longitudinal displacement at the centroid level of the steel beam and y_s is defined in Fig. 6. The adopted bond–slip relationship is reported in Fig. 7, that is:

$$\tau = k_1 \delta \tag{15}$$

According to the stress-based approach, debonding takes place when $|\tau_{\max}| = \tau_p$ and the following relation is derived (see Appendix A):

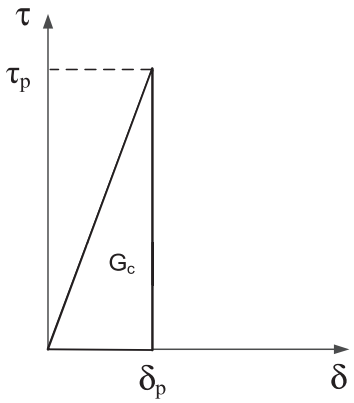

Fig. 7. Linear brittle bond–slip relationship.

$$\tau_p = \frac{M_0 y_s}{b_f f_2 E_s I_s}\left(\lambda + \frac{V_0}{M_0}\right) \tag{16}$$

Considering a simply supported reinforced beam under a three-point bending loading configuration (see Fig. 5), the shear force, V_0, and the bending moment, M_0 at the reinforcement end is given by (see Appendix B):

$$V_0 = \alpha V_0' \qquad \text{and} \qquad M_0 = \alpha M_0' \tag{17}$$

and then, from Eq. (16) and (B1):

$$\tau_p = \frac{\alpha_{\max} y_s}{2 b_f f_2 E_s I_s}(\lambda a + 1) \tag{18}$$

where $\alpha_{\max}$ is the debonding load which is finally equal to:

$$\alpha_{\max} = \frac{2 b_f f_2 E_s I_s}{y_s} \cdot \frac{\tau_p}{\lambda a + 1} \tag{19}$$

Finally, inserting Eq. (11) into Eq. (19) the following expression is achieved for the debonding load:

$$\alpha_{\max} = \frac{2 b_f f_2 E_s I_s}{y_s} \cdot \frac{\tau_p}{1 + \dfrac{\tau_p a}{\sqrt{2 G_c E_f t_f}}} \tag{20}$$

which coincides with Eq. (12). It is important to observe that Eq. (20) was derived in a simpler way compared to Eq. (12) since a brittle linear interface bond–slip law was used and it was not necessary to investigate the full equilibrium path for detecting the debonding load.

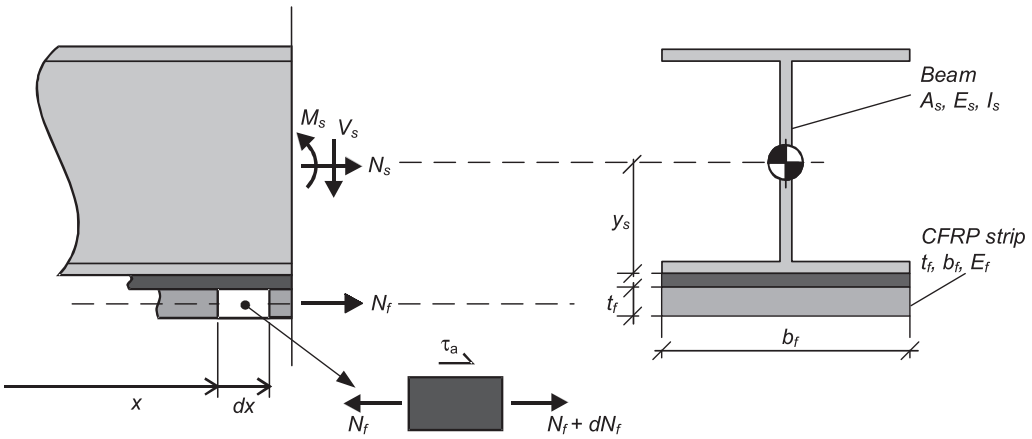

Fig. 6. Simply supported steel beam reinforced with a CFRP plate: notation, stress resultant and free body diagram of an infinitesimal portion of the reinforcing plate.

Eq. (16) can be applied to any loading scheme since it depends only on the bending moment and shear force values at the reinforcement end. In fact, assuming that the external loads increase proportionally to a unit load up to the debonding, one has:

$$\begin{aligned} V_0 &= \alpha V_0' \\ M_0 &= \alpha M_0' \end{aligned} \tag{21}$$

and then from Eq. (16), taking into account that $f_2 = 1/E_f A_f$ and that:

$$\sigma_f = m \cdot \sigma_s = m \cdot \frac{M_0 y_s}{I_s} \tag{22}$$

where $m = E_f/E_s$ is the moduli ratio, it follows:

$$\tau_p = \frac{N_{f,\max}}{b_f}\left(\lambda + \frac{V_0'}{M_0'}\right) \tag{23}$$

where $N_{f,\max}$ is the axial force in the composite strips at debonding. Inserting Eq. (11) in Eq. (23), one has for $N_{f,\max}$:

$$N_{f,\max} = \frac{1}{\frac{1}{\overline{N}_{f,\max}} + \frac{1}{b_f \tau_p}\frac{V_0'}{M_0'}} \tag{24}$$

where

$$\overline{N}_{f,\max} = b_f\sqrt{2G_c E_f t_f} \tag{25}$$

Eq. (24) is the main result of this work. It provides the estimation of the axial force in the composite strips at debonding. It depends not only on the fracture energy, G_c, but also on the maximum shear stress, τ_p. Note that if the effect of the maximum shear stress is neglected, Eq. (24) recovers the formula contained in the design guidelines [39], which is therefore proved to provide a non-conservative estimation of the maximum axial force in the composite strips.

The maximum tensile stress $\sigma_{s,\max}$, in the lower part of the tensile flange of the steel beam is then equal to:

$$\sigma_{s,\max} = \frac{N_{f,\max}}{m \cdot A_f} \tag{26}$$

Finally, using simple strength of materials concepts, the maximum bending moment, $M_{0,\max}$, at the reinforcement end is given by:

$$M_{0,\max} = \left(\sigma_{s,\max} + \frac{N_{f,\max}}{A_s}\right) \cdot \frac{I_s}{y_s} \tag{27}$$

while the load factor at debonding, $\alpha_{\max}$, is given by:

$$\alpha_{\max} = \frac{M_{0,\max}}{M_0'} \tag{28}$$

Eqs. (24)–(28) provide the estimation of the debonding load as long as the expression for M_0' and V_0' are known (see Appendix B).

4. Experimental validation

The validation of the present model is performed by comparing the analytical results with the outcomes of both experimental tests on reinforced steel beams performed at the Material Testing Laboratory of the Politecnico di Milano [40] and of tests from the literature [23].

At the Politecnico di Milano, tests were carried out to characterize the bonding properties of the epoxy resin used in the reinforcement of steel beams. A series of 2500 mm long, H shaped steel beams (HEA 140) was strengthened by bonding a pair of parallel CFRP strips (Sika® CarboDur® M614) to the tension flange and tested under a three-point bending configuration (see Fig. 5). Adhesive type Sikadur® 30 was used to bond the reinforcement to the tension flange. The geometry of the beams and of the reinforcements is reported in Table 1.

Three-point bending tests were performed using the test frame visualized in Fig. 8. The loading was applied with a spherically seated bearing block. Two stiffeners were welded on the beam web in order to prevent crippling at the mid-span section. The reinforced beams were also equipped with lateral supports to prevent lateral torsional buckling that may occur prior to the beam collapse.

The selected steel beam dimensions were representative of typical depth to length ratio and different reinforcing length were considered. In particular, for a reinforcement length equal to 1000 mm, 1250 mm and 1500 mm, the failure mode was due to reinforcement debonding, as shown in Fig. 9. Experimental tests were performed to characterize the mechanical properties of the steel beam, the CFRP strip and the adhesive. Uniaxial tensile tests were performed on coupons cut from the beam flanges and web and an average yield stress of 331 MPa and a tensile strength 469 MPa were obtained, respectively, with a Poisson ratio of 0.3. The CFRP Young's modulus was of 197,000 MPa, while for the adhesive an average Young's modulus of 12,840 MPa and tensile strength of 30.2 MPa were found. The steel Young's modulus was selected equal to 210,000 MPa. Details concerning the materials, specimen preparation and test execution are provided in [40].

Deng and Lee analysed several 1200 mm long UB 127 × 76 × 13 steel beams reinforced with CFRP materials under three-point (see Fig. 5) and four-point (see Fig. 10) loading conditions [23].

Different reinforcing lengths were considered. In particular, for a reinforcement length equal to 300 mm, 400 mm, 500 mm (three-point bending) and 500 mm, 600 mm (four-point bending), the failure mode was due to reinforcement debonding. The steel beam design strength was of 275 MPa and the Young's modulus of 205,000 MPa. Unidirectional epoxy prepreg materials, with a Young modulus of 212,000 MPa, were selected to reinforce the steel beam. Adhesive type Sikadur® 31 was used to bond the rein-forcement to the tension flange. The adhesive shear modulus was 2600 MPa. The geometry of the beams and of the reinforcements is reported in Table 1. Details concerning the materials, specimen preparation and test execution are available in [23].

The analytical failure load of the strengthened beams was determined on the basis of the formulation presented in Section 3. Parameters V_0' and M_0' in Eq. (24) are reported in Appendix B for both the three-point and four-point bending loading configuration. For beams tested in [40] a maximum shear stress τ_p of 20 MPa and a critical fracture energy of 0.11 N/mm were assumed, while for the specimens presented in [23] a maximum shear stress τ_p of 27 MPa and a critical fracture energy of 0.70 N/mm were consid-ered. These values were firstly estimated on the basis of the rela-tionships provided in [37] and then correctly defined following a trial-and-error procedure aimed to minimize the discrepancy between the experimental curves and the analytical results. Differ-ent fracture energy and shear strength values were calibrated since a quite dissimilar surface preparation was adopted in the quoted experimental campaigns. In particular, the parameters related to [23] are in agreement with the experimental results for bonded joints in [30] while the parameters related to [40] represent a lower bound. The end debonding failure load was thus estimated and a good agreement was observed between the results provided by the analytical model and the experimental tests (see Table 1).

5. Numerical validation and parametric analysis

An additional validation of the analytical formulation previously presented (Eqs. (24)–(28)) is performed for different loading

Table 1
Loading configuration and geometry of the tested beams and comparison between the experimental and analytical results.

Specimen reference	Loading mode	Beam length [mm]	Reinforcement geometry [mm × mm × mm]	Experimental failure load [kN]	Analytical failure load [kN]
Fava, 2007 [40]					
B3	Three-point	2500	1500 × 120 × 1.4	114.09	119.45
B4	Three-point	2500	1250 × 120 × 1.4	95.46	96.02
B5	Three-point	2500	1000 × 120 × 1.4	87.71	80.27
Deng and Lee, 2007b [23]					
S303	Three-point	1200	300 × 76 × 3	120.0	119.8
S304	Three-point	1200	400 × 76 × 3	135.0	136.1
S305	Three-point	1200	500 × 76 × 3	149.1	157.7
S405	Four-point	1200	500 × 76 × 3	157.5	157.7
S406	Four-point	1200	600 × 76 × 3	185.5	185.4

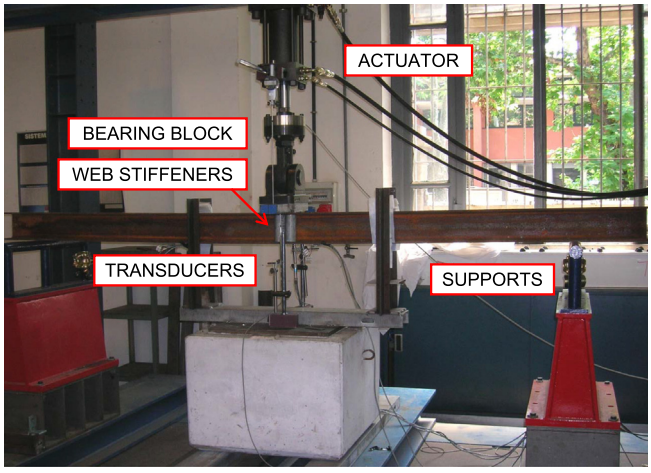

Fig. 8. Three-point bending tests on simply supported reinforced steel beams.

Fig. 9. Detail of the end debonding phenomenon on reinforced steel beam B5 under three-point bending configuration.

schemes through a parametric analysis and the comparison with the results of a numerical procedure recently developed in [34]. In that paper a numerical method, able to follow the complete equilibrium path of a beam externally strengthened by means of FRP sheets up to the complete detachment of the external reinforcement, was proposed.

As observed in [31] and [32], the shape of the cohesive law marginally affects the numerical simulation results, while determining parameters are the maximum shear stress and the area of the bond–slip curve, i.e. the interface strength and the fracture energy. In this work, the exponential cohesive law already used in [31,32] was adopted as well as a standard bilinear bond-slip law.

The response of the externally reinforced beam is numerically derived by enforcing compatibility along the interface between the substrate and the CFRP reinforcement. In view of the softening nature of the interface cohesive law, a displacement controlled numerical procedure was adopted by imposing an increasing displacement δ_m at a certain section and assuming as primary unknowns the interface slips and the external load. It was demonstrated that this approach is stable enough to follow, unless snap-back occurs, the complete equilibrium path from the response of the strengthened beam to that of the bare one after the reinforcement debonding and the consequent sudden load drop.

In the following, the analytical formulation proposed (see Appendix A) is applied, without any loss of generality, to a simply supported beam under different loading configurations. Reference is made to Figs. 11 and 12 where the different loading schemes are presented.

They correspond to parabolic bending moment with linear shear force distribution (Fig. 11) and a cubic bending moment with parabolic shear force (Fig. 12). The proposed analytical model is applied for each loading configuration listed above to evaluate the corresponding end debonding load.

The numerical model summarized above has been used to compute the debonding load for the loading schemes reported in Figs. 11 and 12. Both exponential and bilinear bond-slip laws are used to highlight the potentiality of the analytical formulation. Results are compared to the prevision from Eqs. (24)–(28) in order to validate the analytical approach proposed in this paper.

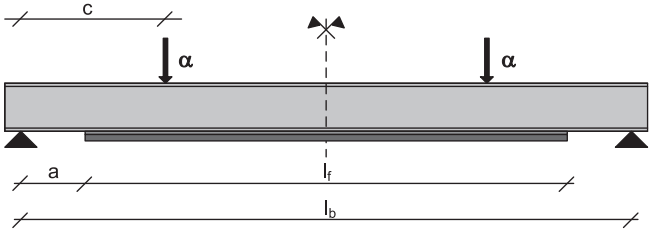

Fig. 10. Simply supported beam under four-point bending loading configuration.

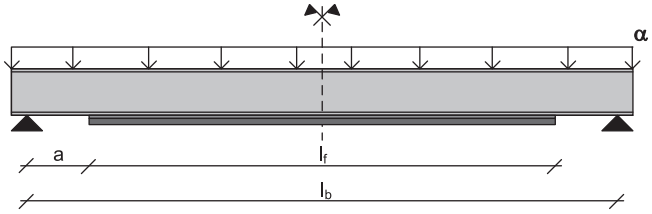

Fig. 11. Simply supported beam under uniformly distributed loading configuration.

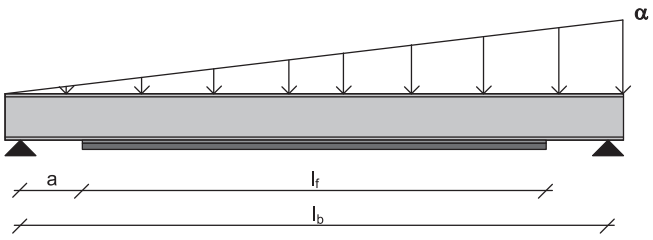

Fig. 12. Simply supported beam under linearly distributed loading configuration.

The beam and reinforcement geometry are reported in Table 2. The selected beam has the same geometry used in [23] for the experimental analysis.

In particular, a beam type UB 127 × 76 × 13 was designated with a beam height equal to 127 mm and a flange width of 76 mm. For the given beam length (l_b = 1100 mm) and reinforcing length (l_f = 500 mm), the distance between the reinforcing end and the beam support is of a = 300 mm. A Young's modulus equal to 210,000 MPa was chosen for the steel beam, while a Young's modulus of 212,000 MPa was selected for the reinforcement. In order to validate the proposed analytical formulation, the debond-ing load was computed according to Eqs. (24)–(28) with reference to the loading configuration represented in Figs. 11 and 12. A frac-ture energy equal to G_c = 0.70 N/mm was considered and a maxi-mum shear stress ranging from 5 MPa to 60 MPa was selected in order to emphasize the effect of this parameter on the debonding load. The failure load was also computed for comparison purposes according to the LEFM solution (see Eq. (1)). From the numerical point of view, the failure load was computed by means of the numerical model summarized above with reference to the bond-slip laws (see Figs. 2 and 3) reported in Eq. (3) (bilinear law) and Eq. (4) (exponential law). In the following, analytical and numeri-cal results are presented and commented in details.

5.1. Uniformly distributed loading configuration

In this case, a uniformly distributed load is considered (see Fig. 11). The shear force is linear in the reinforcement zone and then the failure load is dependent on the maximum shear stress (see Appendix A). The results reported in Fig. 13 show that the LEFM based formula gives a non-conservative estimation of the debonding load while the proposed analytical formulation is in good agreement with the results from the numerical model. Note that the numerical model provides the same failure loads using the bilinear or the exponential bond–slip law.

5.2. Linearly distributed loading configuration

In this case, a linearly distributed load is considered (see Fig. 12). The shear force is parabolic in the reinforcement zone and then the failure load depends also on the maximum shear stress (see Appendix A). The results reported in Fig. 14 show that the LEFM based formula gives a non-conservative estimation of the debonding load while the proposed analytical formulation is in good agreement with the results of the numerical model, which provides, as in the previous case, the same failure loads using the bilinear or the exponential bond–slip law.

Table 2
Specimen and reinforcement geometry used in the parametric analysis.

Setup geometry	
L_b = 1100 mm	L_f = 500 mm
Beam UB 127 × 76 × 13	
A_s = 1652 mm^2	I_s = 4.73E+06 mm^2
Reinforcement geometry	
t_f = 3 mm	b_f = 76 mm

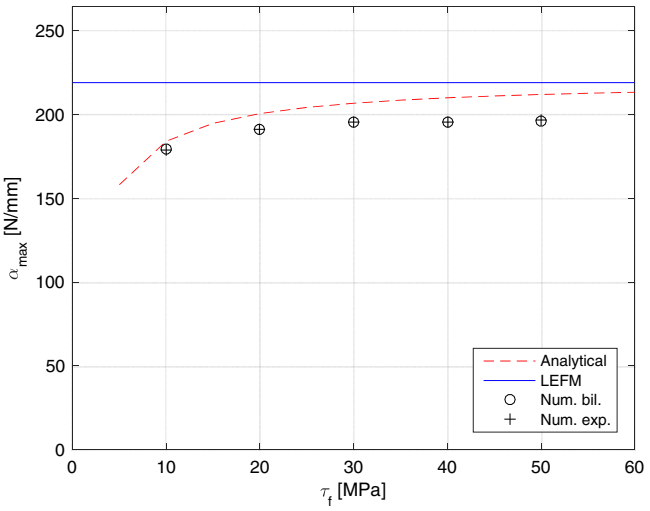

Fig. 13. Debonding load versus maximum shear stress of the bond–slip law for uniformly distributed loading configuration.

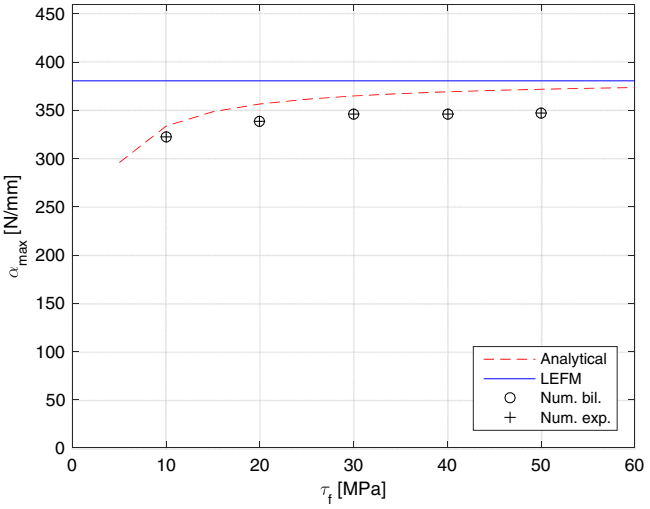

Fig. 14. Debonding load versus maximum shear stress of the bond–slip law for linearly distributed loading configuration.

6. Conclusions

In this paper an analytical formulation for the prediction of the edge debonding in FRP plated steel beams was presented. In the literature several methods already exist for the evaluation of the end debonding failure in strengthened steel beams and both linear and non-linear effects at the interface are taken into account. Nonetheless, such models often lead to difficult, cumbersome and time-consuming calculation efforts. For this reason, the presented approach makes use of a simplified energy-based debonding criterion. It is assumed that only shear stresses are transmitted at the interface. Besides, a local approximation of the shear stresses at the reinforcing ends is introduced, providing a simplified design formula for the edge debonding.

This is the main novelty of this work since the proposed formulation is straightforwardly applicable in the design phase of rein-

forced steel beams with a generic structural configuration and loading scheme, providing a reliable and simple estimation of the end debonding strength. The model is also able to capture the most critical and relevant aspects of the debonding phenomenon. As an example, the dependency of the bond strength from the maximum shear stress of the bond-slip law is clearly detected.

The validation of the model is performed by comparing the analytical results with the outcomes of experimental tests on reinforced steel beams with different beam lengths and reinforcement geometries and tested both under three-point and four-point loading configurations. An extremely good agreement was observed.

Numerical simulations were also performed using a recently proposed method. It was observed that the analytical results are in good agreement with the numerical ones. Additionally, the debonding strength is not dependent from the shape of the bond–slip law while the so-called LEFM approach provides non-conservative estimations of the bond strength. This is a proof of the potentialities of the proposed analytical formulation which can be finally used to develop a more refined design method for beam strengthening.

Acknowledgements

The financial support of the Politecnico di Milano – Italy is gratefully acknowledged.

Appendix A

According to Fig. 6, the equilibrium of an infinitesimal portion of the composite strip reads:

$$\frac{dN_f}{dx} + \tau \cdot b_f = 0 \tag{A1}$$

where τ is the shear stress, while N_f is the axial force in the compos-ite strip. On the other hand, the equilibrium equations of the rein-forced steel beam read (see Fig. 8):

$$N = N_s + N_f \quad \text{and} \quad M = M_s + N_f \cdot z \tag{A2}$$

where N and M are the external axial force and bending moment applied to a given section of the reinforced composite beam, respectively, and z is the distance between the centroids of steel and reinforcement sections. The constitutive relationships for the steel beam and the composite strips are:

$$N_f = E_f A_f \frac{du_f}{dx},\ N_s = E_s A_s \frac{du_s}{dx},\ M_s = E_s I_s \frac{d\psi_s}{dx} \tag{A3}$$

The adopted bond–slip relationship is reported in Fig. 7, that is $\tau = k_1 \delta$.

Differentiating Eq. (14) and inserting the constitutive relationships (see Eq. (A3)), one gets:

$$\frac{d\delta}{dx} = \frac{N_s}{E_s A_s} + \frac{M_s}{E_s I_s} y_s - \frac{N_f}{E_f A_f} \tag{A4}$$

Inserting Eq. (A2) into Eq. (A4), after some algebra, the following relationship is found:

$$\frac{d\delta}{dx} + f_2 N_f = \frac{N}{E_s A_s} + \frac{M}{E_s I_s} y_s \tag{A5}$$

where, since the axial and bending stiffness of the steel beam are much greater than the reinforcement axial stiffness, one has:

$$f_2 = \frac{1}{E_s A_s} + \frac{z \cdot y_s}{E_s I_s} + \frac{1}{E_f A_f} \simeq \frac{1}{E_f A_f} \tag{A6}$$

Edge debonding is triggered by a stress concentration close to the reinforcement end and then propagates toward the middle of the beam. For this reason, a simple and reliable analytical solution of the debonding load can be obtained through a linear approximation of the right hand side of Eq. (A5) centred at the reinforcement end:

$$\frac{N}{E_s A_s} + \frac{M}{E_s I_s} y_s \simeq \frac{N_0}{E_s A_s} + \frac{M_0 + V_0 \cdot x}{E_s I_s} y_s = \Delta\varepsilon_0 + \Delta\varepsilon_1 x \tag{A7}$$

with:

$$\Delta\varepsilon_0 = \frac{N_0}{E_s A_s} + \frac{M_0}{E_s I_s} y_s \quad \text{and} \quad \Delta\varepsilon_1 = \frac{V_0}{E_s I_s} y_s \tag{A8}$$

In Eqs. (A7) and (A8), N_0, V_0 and M_0 are the axial force, shear force and bending moment at the reinforcement end, respectively. The above local approximation of the stress field close to the edge debonding provides a very useful simplification of the governing equations. Eq. (A5) now reads:

$$\frac{d\delta}{dx} + f_2 N_f = \Delta\varepsilon_0 + \Delta\varepsilon_1 x \tag{A9}$$

Differentiating Eq. (A9) and inserting Eqs. (A1) and (15), the fol-lowing second order differential equation is obtained for the rela-tive displacement δ:

$$\frac{d^2\delta}{dx^2} - \lambda^2 \delta = \Delta\varepsilon_1 \tag{A10}$$

where

$$\lambda^2 = f_2 k_1 b_f \tag{A11}$$

Note that Eq. (A11) coincides with Eq. (10). Besides, from Eq. (8) one has:

$$k_1 = \frac{\tau_p^2}{2G_c} \tag{A12}$$

and

$$\lambda = \frac{\tau_p}{\sqrt{2G_c E_f t_f}} \tag{A13}$$

Since the relative displacement δ rapidly decreases and $N_f = N_{f0}$ at the reinforcement end (prescribed tensile force at the reinforcement end), the solution of Eq. (A10), for a sufficiently long reinforcement strips, reads:

$$\delta = \frac{1}{\lambda}(f_2 N_{f0} - \Delta\varepsilon_0) e^{-\lambda x} - \Delta\varepsilon_1 \frac{1}{b_f k_1 f_2} \tag{A14}$$

while the following expression is achieved for the shear stress, τ,(see Eq. (15)):

$$\tau = \frac{1}{b_f}\left[\left(N_{f0} - \frac{\Delta\varepsilon_0}{f_2}\right)\lambda e^{-\lambda x} - \frac{\Delta\varepsilon_1}{f_2}\right] \tag{A15}$$

The maximum shear stress, τ_{max}, is achieved at $x = 0$ and then:

$$\tau_{max} = \frac{1}{b_f}\left[\left(N_{f0} - \frac{\Delta\varepsilon_0}{f_2}\right)\lambda - \frac{\Delta\varepsilon_1}{f_2}\right] \tag{A16}$$

In the following, the case $N_{f0} = 0$ is considered, that is no axial force is applied to the reinforced steel beam and then, taking into account Eq. (A8):

$$\tau_{max} = -\frac{y_s}{b_f f_2 E_s I_s}(\lambda M_0 + V_0) \tag{A17}$$

Appendix B

In the following the shear force and bending moment at the reinforcement end are provided for the loading schemes consid-

ered in experimental and numerical validation of the proposed formulation.

B.1. Three-point bending

The loading scheme is reported in Fig. 5 and, in this case, one has for V'_0 and M'_0:

$$\begin{aligned} V'_0 &= \frac{1}{2} \\ M'_0 &= \frac{a}{2} \end{aligned} \tag{B1}$$

where a is given in Fig. 8.

B.2. Four-point bending

The loading scheme is reported in Fig. 10 and, in this case, one has for V'_0 and M'_0:

$$\begin{aligned} V'_0 &= 1 \\ M'_0 &= a \end{aligned} \tag{B3}$$

where a is given in Fig. 10.

B.3. Uniformly distributed loading

The loading scheme is reported in Fig. 11 and, in this case, one has for V'_0 and M'_0:

$$\begin{aligned} V'_0 &= \left(\frac{l_b}{2} - a\right) \\ M'_0 &= \frac{a}{2}(l_b - a) \end{aligned} \tag{B4}$$

where a and l_b are given in Fig. 11.

B.4. Linearly distributed loading

The loading scheme is reported in Fig. 12 and, in this case, one has for V'_0 and M'_0:

$$\begin{aligned} V'_0 &= -\left(\frac{l_b}{6} - \frac{(l_b - a)^2}{2l_b}\right) \\ M'_0 &= \frac{(l_b - a)}{6} \cdot \left(l_b - \frac{(l_b - a)^2}{l_b}\right) \end{aligned} \tag{B5}$$

where a and l_b are given in Fig. 12.

References

[1] Saadatmanesh H. Extending service life of concrete and masonry structures with fiber composites. Constr Build Mater 1997;11:327–55.
[2] Hollaway LC. The evaluation of and the way forward for advanced polymer composites in the civil infrastructure. Constr Build Mater 2003;17:365–78.
[3] Hollaway LC, Cadei J. Progress in the technique of upgrading metallic structures with advanced polymer composites. Prog Struct Mat Eng 2002;4(2):131–48.
[4] Zhao XL, Zhang L. State of the art review on FRP strengthened steel structures. Eng Struct 2007;29(8):1808–23.
[5] Teng JG, Yu T, Fernando D. Strengthening of steel structures with fiber-reinforced polymer composites. J Constr Steel Res 2012;78:131–43.
[6] Bocciarelli M. Response of statically determined steel beams reinforced by CFRP plates in the elastic–plastic regime. Eng Struct 2009;31:956–67.
[7] Tavakkolizadeh M, Saadatmanesh H. Fatigue strength of steel girders strengthened with carbon fiber reinforced polymer patch. J Struct Eng 2003;129(2):186–96.
[8] Jones SC, Civjan SA. Application of fibre reinforced polymer overlays to extend steel fatigue life. J Compos Constr 2003;7(4):331–8.
[9] Nozaka K, Shield CK, Hajjar JF. Effective bond length of carbon-fiber-reinforced polymer strips bonded to fatigue steel bridge I-girders. J Bridge Eng 2005;10(2):195–205.
[10] Colombi P. Plasticity induced fatigue crack growth retardation model for steel elements reinforced by composite patch. Theoret Appl Fract Mech 2006;43:63–76.
[11] Deng J, Lee MMK. Fatigue performance of metallic beam strengthened with a bonded CFRP plate. Compos Struct 2007;78:222–31.
[12] Kim YJ, Harries KA. Fatigue behaviour of damaged steel beams repaired with CFRP strips. Eng Struct 2011;33(5):1491–502.
[13] Ghafoori E, Motavalli M, Botsis J, Herwig A, Galli M. Fatigue strengthening of damaged metallic beams using prestressed unbonded and bonded CFRP plates. Int J Fatigue 2012;44:303–15.
[14] Colombi P, Fava G. Experimental study on the fatigue behaviour of cracked steel beams repaired with CFRP plates. Eng Fract Mech 2015;145:128–42.
[15] Ghafoori E, Motavalli M, Nussbaumer A, Herwig A, Prinz GS, Fontana M. Design criterion for fatigue strengthening of riveted beams in a 120-year-old railway metallic bridge using pre-stressed CFRP plates. Compos B 2015;68:1–13.
[16] Cadei JMC, Stratford TJ, Hollaway LC, Duckett WH. C595-Strengthening metallic structures using externally bonded fibre-reinforced composites. London: CIRIA; 2004.
[17] Schnerch D, Dawood M, Rizkalla S, Sumner E. Proposed design guidelines for strengthening of steel bridges with FRP materials. Constr Build Mater 2007;21:1001–10.
[18] Colombi P, Poggi C. An experimental, analytical and numerical study of the static behaviour of steel beams reinforced by pultruded CFRP strips. Compos B 2006;37:64–73.
[19] Pellegrino C, Maiorana E, Modena C. FRP strengthening of steel and steel-concrete composite structures: an analytical approach. Mater Struct 2009;42:353–63.
[20] Linghoff D, Al-Emrani M, Kliger R. Performance of steel beams strengthened with CFRP laminate – part 1: laboratory tests. Compos B 2010;41:509–15.
[21] Bocciarelli M, Colombi P. On the elasto-plastic behavior of continuous steel beams reinforced by bonded CFRP lamina. Eng Struct 2013;49:756–66.
[22] Stratford T, Cadei J. Elastic analysis of adhesion stresses for the design of a strengthening plate bonded to a beam. Constr Build Mater 2006;20:34–45.
[23] Deng J, Lee MMK. Behaviour under static loading of metallic beams reinforced with a bonded CFRP Plate. Compos Struct 2007;78:232–42.
[24] Yu Y, Chiew SP, Lee CK. Bond failure of steel beams strengthened with FRP laminates – Part 2: verification. Compos B 2011;42:1122–34.
[25] Rabinovitch O. Fracture-mechanics failure criteria for RC beams strengthened with FRP strips – a simplified approach. Compos Struct 2004;64:479–92.
[26] Colombi P. Reinforcement delamination of metallic beams strengthened by FRP strips: fracture mechanics based approach. Eng Fract Mech 2006;73:1980–95.
[27] Carpinteri A, Cornetti P, Pugno N. Edge debonding in FRP strengthened beams: stress versus energy failure criteria. Eng Struct 2009;31:2436–47.
[28] De Lorenzis L, Paggi M, Carpinteri A, Zavarise G. Linear elastic fracture mechanics approach to plate end debonding in rectilinear and curved plated beams. Adv Struct Eng 2010;13(5):875–89.
[29] Xu XP, Needleman A. Numerical simulation of fast crack growth in brittle solids. J Mech Phys Solids 1994;42:1397–434.
[30] Bocciarelli M, Colombi P, Fava G, Poggi C. Prediction of debonding strength of tensile steel/CFRP joints using fracture mechanics and stress based criteria. Eng Fract Mech 2009;76:299–313.
[31] Bocciarelli M, Colombi P, Fava G, Poggi C. Interaction of interface delamination and plasticity in tensile steel members reinforced by CFRP plates. Int J Fract 2007;146:79–92.
[32] Bocciarelli M, Colombi P. Elasto-plastic debonding strength of tensile steel/CFRP joints. Eng Fract Mech 2012;85:59–72.
[33] Yuan H, Teng JG, Seracino R, Wu ZS, Yao J. Full-range behavior of FRP-to-concrete bonded joints. Eng Struct 2004;26:553–65.
[34] Bocciarelli M, Pisani MA. Modified force method for the nonlinear analysis of FRP reinforced concrete beams. Compos Struct 2015;131:645–53.
[35] Cornetti P, Corrado M, De Lorenzis L, Carpinteri A. An analytical cohesive crack modeling approach to the edge debonding failure of FRP-plated beams. Int J Solids Struct 2015;53:92–106.
[36] De Lorenzis L, Zavarise G. Cohesive zone modelling of interfacial stresses in plated beams. Int J Solids Struct 2009;46:4181–91.
[37] Teng JC, Fernando D, Yu T. Finite element modelling of debonding failures in steel beams flexurally strengthened with CFRP laminates. Eng Struct 2015;86:213–24.
[38] Broek D. Elementary engineering fracture mechanics. Nordhoff International Publishing; 1982.
[39] CNR-DT 200 R1/2013. Istruzioni per la progettazione, l'esecuzione e il controllo di interventi di consolidamento statico mediante l'utilizzo di compositi fibrorinforzati. Materiali, strutture di c.a. e di c.a.p., strutture murarie (in Italian). Italian National Research Council; 2013.
[40] Fava G. Strengthening of metallic structures using carbon fiber reinforced polymer materials Ph.D. thesis. Politecnico di Milano – Department of Structural Engineering, 2007.